Available online at www.sciencedirect.com
SCIENCE DIRECT
Journal of Power Sources 157 (2006) 377–384
JOURNAL OF POWER SOURCES
www.elsevier.com/locate/jpowsour

Electrical behaviour of glass–ceramics in the systems RO–BaO–SiO_2 (R = Mg, Zn) for sealing SOFCs

C. Lara [a], M.J. Pascual [a], R. Keding [b], A. Durán [a,*]

[a] *Instituto de Cerámica y Vidrio (CSIC), Glasses, Kelsen 5, Campus de Cantoblanco, 28049 Madrid, Spain*
[b] *Otto-Schott Institut, Fraunhoferstrasse 6, 07743 Jena, Germany*

Received 21 June 2005; received in revised form 28 July 2005; accepted 31 July 2005
Available online 25 October 2005

Abstract

The electrical behaviour of glass–ceramics in the system, RO–BaO–SiO_2 (R = Mg, Zn), was characterised in the range from 500 to 850 °C by electrochemical impedance spectroscopy (EIS) simulating the start-up thermal treatment programme of an SOFC. The thermal treatment covers the sintering and crystallisation temperature range of the glass–ceramics. Over the whole temperature range, samples presented an electrical resistance much higher than 10^4 Ω cm, thus behaving like insulators. Impedance spectra were expressed as Bode plots showing the impedance as a function of frequency and phase angle. Electrical properties corresponding to the bulk specimen were obtained by employing an equivalent circuit to simulate the impedance spectra. The influence of crystallisation on electrical properties has been followed by EIS showing the capability of this method as a thermal analysis technique.

The specific conductivities were illustrated by Arrhenius plots and its derivative ($-\mathrm{d}\log\sigma/\mathrm{d}(1/T)$). Glass transition and crystallisation processes strongly affect the derivative, whose shape can provide information about both processes. Hot-stage microscopy (HSM) and differential thermal analysis (DTA) were carried out under the same thermal conditions. The results obtained by the different techniques were analysed in detail resulting in good agreement.

Keywords: Glass–ceramic sealant; SOFC; Electrical behaviour; Electrochemical impedance spectroscopy; Thermal analysis

1. Introduction

Planar solid oxide fuel-cells (SOFCs) are electrochemical devices that directly convert the chemical energy of several gas fuels into electricity [1]. In order to prevent fuel and oxidant gas leakages at operating temperatures, gas-tight seals must be applied along the edges of the cells and between the stack and the gas manifolds. The sealing material will therefore be in contact with the stack components, especially the electrolyte (YSZ) and interconnect material (stainless steel or other alloys), during operation around 850 °C. The sealing material must fulfil a number of requirements. It should have a thermal expansion coefficient (CTE) that matches those of the fuel-cell components ($9–12 \times 10^{-6}\ \mathrm{K}^{-1}$), a high chemical compatibility with the joining materials, and high chemical stability in reducing and oxidising environments [2,3]. To enable formation of a stable stack, the sealant must also not spread to the fuel-cell components [4]. Furthermore, it should have a suitable viscosity at the operating temperature to be able to absorb stresses and withstand overpressures [5].

In addition, a high electrical resistance ($\rho > 10^4$ Ω cm, that is $\sigma < 10^{-4}\ \mathrm{S\,cm}^{-1}$) is one of the most important requirements. Otherwise, current leakages would take place rendering short circuits and leading to a noticeable decrease in the electrical efficiency of the fuel-cells, also bringing about electrolytic damage [6].

Glasses and glass–ceramics seem to be the most appropriate materials to fulfil these stringent requirements. Thus, several studies have been conducted focused on the application of these materials as suitable sealants for SOFCs [2,7–10].

The EIS technique has been widely used for the study of the electrical behaviour of glasses containing alkaline ions [11–15]. However, only a few publications deal with electrical characterisation of alkali-free silicate glasses [16–20].

* Corresponding author. Tel.: +34 91 735 58 40/57; fax: +34 91 735 58 43.
E-mail addresses: lopez@icv.csic.es (C. Lara), mpascual@icv.csic.es (M.J. Pascual), cai@rz.uni-jena.de (R. Keding), aduran@icv.csic.es (A. Durán).

0378-7753/$ – see front matter © 2005 Elsevier B.V. All rights reserved.
doi:10.1016/j.jpowsour.2005.07.084

In most oxide glasses, the electrical conductivity results from ionic mobility. This conductivity is proportional to the concentration of the charge carrier ions and to their mobility or diffusion coefficients. In most commercial glasses alkaline ions are the main charge carriers. However, the conduction mechanism in various "alkali-free" silicate glasses containing earth-alkaline ions is unknown. In barium silicate glasses with 30 and 50 mol% barium oxide, Evstrop'ev and Kharyuzov [16] found that the diffusion coefficient of barium ions and the electrical conductivity obeyed Einstein's Eq. (1)

$$\sigma = \frac{Z^2 F^2 Dc}{RT} \quad (1)$$

where Z is the ionic charge, F the Faraday constant, D the diffusion coefficient, c the concentration, R the gas constant and T is the temperature.

On the other hand, in calcium silicate glasses the diffusion coefficient of Ca^{2+} is too low to account for the electrical conductivity [18]. In this case, the diffusion coefficients of monovalent cations cannot be described by considering the glass to be a viscous liquid but like a rigid solid with mobile interstitial ions.

Zarzycki pointed out that the co-ordination numbers of cations in silicates can vary widely [17]. If large amounts of alkaline earth ions are present, the anionic part of the glass must also vary. For example, rings or chains may predominate in different systems. The detailed structure of the glass, and not simply a random distribution of cations, must therefore play an important role in ionic conduction.

Electronic conduction in oxide glasses is usually attributed to transition metal ions. The composition of the glasses studied in this work rules out an electronic process. Likewise, oxygen diffusion is also considered unlikely for these glasses.

The EIS technique not only measures electrical conductivity, but is also useful to monitor sintering and crystallisation processes, as much in glasses [14,21,22] as in other materials [23].

The sealing of SOFCs is usually carried out by paste technology with powdered glass. Thus, for obtaining a final dense and gas-tight glass–ceramic seal, sintering should be completed before crystallisation takes place. It is important, therefore, to determine the critical temperatures for these processes. Viscous flow is the dominant mechanism in glass sintering [24]. During sintering there are two contributions to the resistivity, one due to glass powder and the other to the porosity. It is common knowledge that in most cases, pores have an electrical conductivity several orders of magnitude lower than that of the glass [14].

On the other hand, if microstructural changes take place during the heating process, they should be reflected in the electrical measurements, since the electrical conductivity depends on the composition and volume of the phases. If compositional changes take place, for example, because of crystallisation, the conductivity must also change. Hence, the critical temperature for these processes could be detected by a change in the conductivity. In samples that undergo a phase transition, the slope in the Arrhenius plot ($-\mathrm{d}\log\sigma/\mathrm{d}(1/T)$) is a sensitive measure for detecting this, changing if the activation energy of the electrical conductivity of the initial and the final phases are different. Therefore, EIS could also be useful to determine T_g, sintering, crystallisation and even melting temperatures [22].

In this work, EIS technique was used to study the electrical behaviour of some compositions in the MgO–BaO–SiO_2 and ZnO–BaO–SiO_2 systems from 500 to 850 °C. The studied compositions have been advanced as possible candidates as sealant glass–ceramics for SOFCs [10]. Another goal of the work was to verify the validity and reproducibility of EIS as a thermal analysis technique when applied to these glasses. The influence of sintering and crystallisation processes on the electrical properties was investigated. For purposes of comparison, differential thermal analysis (DTA) and densification measurements followed by hot-stage microscopy (HSM) were carried out under the same thermal conditions. Dynamic high temperature X-ray diffraction (HTXRD) was used to characterise the crystalline phases formed during the sealing process.

2. Experimental

2.1. Sample preparation

Two glass compositions with the same BaO/RO = 1.5 (R = Mg and Zn) and different SiO_2 contents were studied: $50SiO_2{\cdot}30BaO{\cdot}20ZnO$ (Zn1.5–50) and $55SiO_2{\cdot}27BaO{\cdot}18MgO$ (Mg1.5–55) (mol%). These compositions exhibit good thermal properties (CTE = 9.5–11 $\pm$ 0.1 $\times 10^{-6}\,K^{-1}$) and a sintering/crystallisation behaviour, which produces high relative densities [10]. These properties are crucial factors in obtaining a thermally stable, dense and homogeneous seal.

Batch compositions calculated to yield 25 g of glass were prepared from reagent grade $BaCO_3$, $MgCO_3$, ZnO and silica sand with low Fe_2O_3 content. The batches were melted in Pt crucibles in an electrical furnace at 1600 °C for 2 h and cast in brass moulds in air. The glasses were ground in a ball agate mill and subsequently sieved under a 20 μm mesh. The average particle size, determined by laser scattering with a Mastersizer S instrument (Malvern Instruments Ltd.), was 10 μm.

2.2. HSM, DTA and HTXRD

The sintering and crystallisation processes of powdered glass compositions (particle size diameter $\phi < 20$ μm) were followed by HSM and DTA. HSM was carried out with a hot-stage microscope EM 201 with image analysis system and Leica electrical furnace 1750/15 on small uniaxially pressed specimens (3 mm in height and ~3 mm in diameter) positioned onto Al_2O_3 plates (>99.5%). The microscope projects the image of the sample through a quartz window and onto the recording device. The computerised image analysis system automatically records and analyses the geometry changes of the sample during heating. The temperature was measured with a Pt/Rh thermocouple in contact with the alumina plate. The measurements were conducted in air with heating rates of 2 and 5 °C min^{-1} up to a maximum temperature of 950 °C. Densification curves were obtained from the HSM results. The HSM software calculates the percentage of decrease in height, width and area of the sample images with respect to the initial dimensions of the samples, such that the

densification as a function of temperature or time may be calculated. The relative density of cylindrical samples (density of the sample divided by the bulk glass density) during sintering can be obtained by

$$\rho_r = \left(\frac{h_r}{A_r^2}\right)\rho_0 \quad (2)$$

in which h_r is the relative height and A_r is the relative area of the samples at any temperature or time, and ρ_0 is the initial relative density of the green sample (relative to the bulk glass density). The initial relative green density of the samples was around 0.60.

DTA tests were performed in air with an EXSTAR 6300 (Seiko) instrument employing approximately 50 mg of glass powder ($\phi < 20\,\mu m$). Pt crucibles were used as sample holders and α-Al_2O_3 calcined at 1200 °C as inert reference. The heating rates were again 2 and 5 °C min^{-1} to 1100 °C.

HTXRD patterns were carried out on powder samples at a heating rate of 2 °C min^{-1} from 600 °C up to 850 °C, followed by equilibration at this temperature for 15 h and cooling. One diffractogram was recorded each 50 °C allowing the sample to thermally stabilise; three more were taken at 850 °C after 1, 5 and 15 h, and the last one at room temperature after cooling. The equipment used was a Philips 1710 generator, vacuum (3–5 × 10^{-3} bar) with platinum slides as sample support.

2.3. EIS measurements

Disk pellets of 10 mm diameter and thickness, around 2 mm, were obtained by uniaxial pressing of glass particles. The initial relative green densities were around 0.55–0.65. The conductivity of these samples was measured using a Zahner IM5d impedance analyser in a frequency range from 0.1 Hz to 1 MHz with a cell shown in Fig. 1. The samples were inserted between two platinum disks with a diameter of 12 mm. Each disk was connected by two Pt-wires (diameter: 0.35 mm). Alumina tubes were used to apply a small force necessary to keep the platinum disks in contact with the glass sample. The ac-amplitude used was 50 mV, with no dc bias. The potentiostat was connected to the sample as displayed in Fig. 1. To establish the contact, the samples were heated to 600 °C and then cooled at 10 °C min^{-1}. After this procedure, the samples were subjected to different cycles of heating and cooling from 400 °C to near the glass transition temperature (T_g) at a heating rate of 10 °C min^{-1}, an impedance spectrum was recorded every 40 or 50 °C. The spectra were fitted using an appropriate equivalent circuit (with Thales simulation software, Zahner Elektrik, Kronach, Germany).

In another series of experiments, the impedance was measured at a constant frequency from ~500 °C to 850 °C at a heating rate of 2 and 5 °C min^{-1}, again with an isothermal stage at 850 °C for 15 h, followed by cooling at the same cooling rates. This procedure was adopted in order to simulate the initial and final working conditions of an SOFC. The constant frequency was adjusted to a value attributed to a phase angle of 0° (phase angle dominated by the resistive part of the sample), which was obtained from the previously recorded impedance spectra at temperatures close to T_g. All measurements were carried out in a dc-powered electrical furnace controlled by a EUROIIERM temperature controller with an absolute error of ±2 °C. Impedances lower than 100 MΩ were measured with an accuracy of ±0.5%.

After the impedance measurements were completed, XRD-patterns were recorded (using a Siemens D5000 diffractometer) from powdered samples of the final glass–ceramics.

3. Results and discussion

3.1. Sintering/crystallisation process

DTA and densification plots on the same temperature scale allow the thermal behaviour of samples subjected to sintering and devitrification phenomena to be evaluated. Fig. 2 presents these results for a Zn1.5–50 sample at a heating rate of 5 °C min^{-1}. In the figure, T_g is the glass transition temperature, T_x the onset crystallisation temperature (on heating), T_c the maximum crystallisation temperature, T_{FS} the temperature of first shrinkage and T_{MS} the temperature of the maximum shrinkage reached. The first shrinkage temperatures correspond to the average temperature of the temperature range in which the first 10% of densification is reached, and the maximum shrinkage temperature corresponds to the average temperature of the temperature range in which densifica-

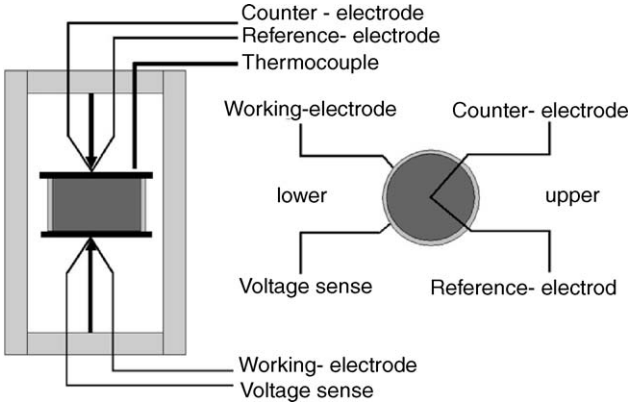

Fig. 1. Scheme of the electrical cell used for EIS measurements.

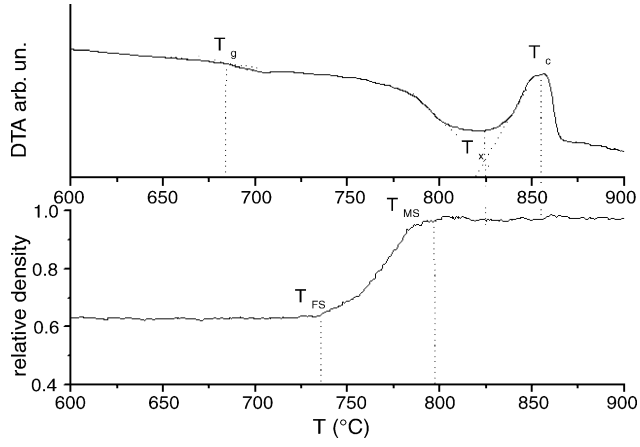

Fig. 2. DTA and HSM plots of Zn1.5–50 powdered glass at 5 °C min^{-1}.

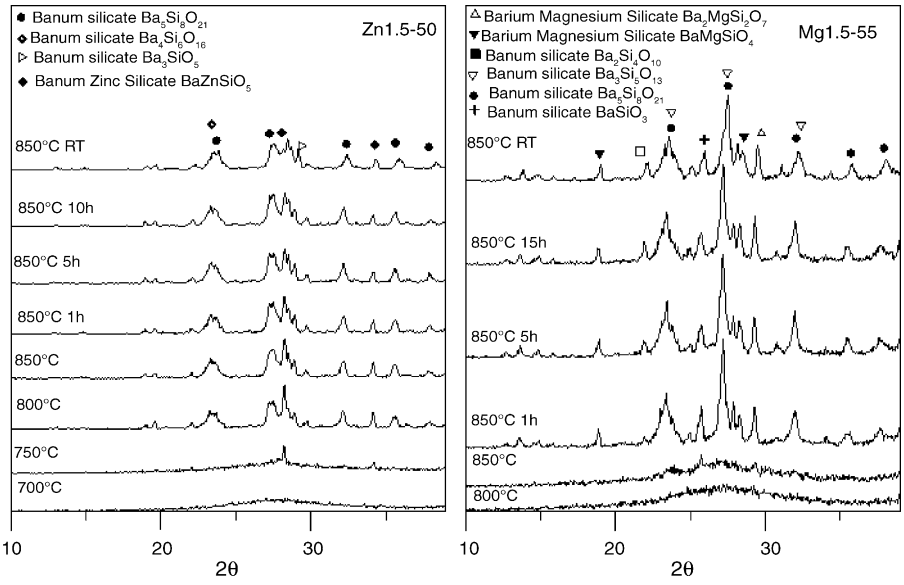

Fig. 3. HTRXD for Zn1.5–50 and Mg1.5–55 carried out in air at 2 °C min^{-1} and at 850 °C during different times.

tion is up to 10% below the maximum densification reached [9,25].

The plot of the relative density as a function of temperature (according Eq. (2)) shows a sintering process, which starts at around 735 °C and is completed around 800 °C. At higher temperatures, once the maximum sintering has been reached, a further increase of temperature no longer influences the densification process. The DTA plot shows that crystallisation starts (T_x = 830 °C) after the material has reached the maximum density; T_x falls in the stage where shrinkage has finished at about 830 °C. Under these conditions, a dense crystallised material is obtained. Similar behaviour is observed for the Mg1.5–55 composition.

The thermal data obtained by DTA and HSM of both compositions at the different heating rates are reported in Table 1.

The difference $T_x - T_{MS}$ may be assumed to be an empirical parameter of sinterability and is higher when the ability for sintering versus crystallisation is better [10]. It has been observed for different glass compositions [10] that, for $T_x - T_{MS} \geq 20$, sintering and crystallisation processes are separated enough to result in dense glass–ceramics. Viscous flow allows densification and is hindered with the presence of the first crystals. For example, Zn1.5–50 heated at 2 °C min^{-1} showed a lower densification in the HSM experiment, with corresponding $T_x - T_{MS}$ values lower than 20, due to a greater nucleation in these conditions.

Table 1
DTA and HSM temperatures

T (°C)	Zn1.5–50		Mg1.5–55	
	2 °C min^{-1}	5 °C min^{-1}	2 °C min^{-1}	5 °C min^{-1}
T_g (DTA)	676 ± 7	684 ± 7	684 ± 7	708 ± 7
T_{FS} (HSM)	723 ± 5	735 ± 5	748 ± 5	757 ± 5
T_{MS} (HSM)	788 ± 5	797 ± 5	800 ± 5	819 ± 5
T_x (DTA)	796 ± 9	830 ± 9	835 ± 9	852 ± 9
T_c (DTA)	830 ± 9	854 ± 9	863 ± 9	877 ± 9
$T_x - T_{MS}$	8	33	35	33

Fig. 3 shows the HTXRD patterns for Zn1.5–50 and Mg1.5–55. No significant crystallisation was observed in Zn1.5–50 until the appearance of barium zinc silicate at 750 °C. Further crystallisation results in the formation of different barium silicates. For Mg1.5–55, crystallisation is detected after 1 h at 850 °C; the main crystalline phases are barium silicates and barium magnesium silicates. Barium silicates exhibit a CTE ∼12–14 × 10^{-6} K^{-1}, which is within the range required for SOFC operation.

3.2. Electrical conductivity

In a first set of EIS tests, the electrical conductivity was measured from 400 °C to temperatures close to T_g. A typical impedance spectrum obtained over a frequency range of 0.1 Hz–1 MHz is shown in Fig. 4 for Mg1.5–55 at 640 °C (Bode diagram), depicting the logarithm of absolute values of the

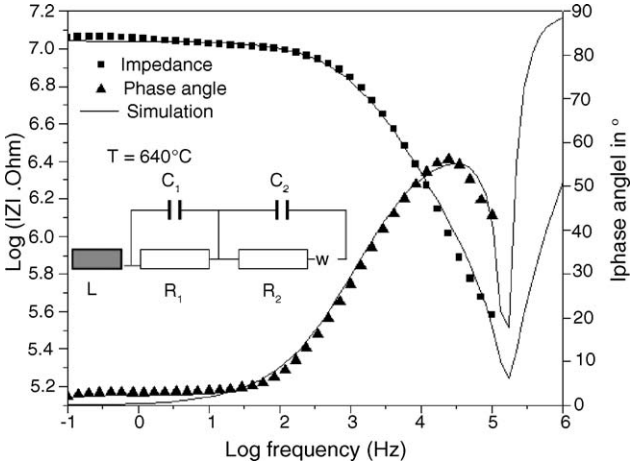

Fig. 4. Bode plot recorded at 640 °C for sample Mg1.5–55.

impedance, $|Z|$, and the absolute value of phase angle $|\varphi|$ as a function of logarithm of frequency.

The equivalent circuit, also shown in Fig. 4, was used for numerical analysis of the experimental spectra. It is composed of an inductance L attributed to the wiring, a resistivity R_1 in parallel to a capacitance C_1, both representing the bulk properties of the studied samples (C_1 is also affected by the scattering capacitance of the experimental set up) and the resistivity R_2, the capacitance C_2 and the Warburg impedance W, which represent phenomena occurring at the electrode/sample interface. These parameters describe the kinetics of the electron-transfer reactions, the electrochemical double layer and the diffusion of redox active species to and from the surface of the electrodes, and were not used for further analyses and discussion. The simulated values are represented by the solid line in Fig. 4. All impedance spectra could be simulated with high accuracy, with a maximum error of ±5%. The procedure was the following: each impedance element was set to a certain value and subjected to an iterative approximation until the final values were obtained.

At low frequency, the phase angles are close to 0°, i.e. the samples act as pure resistors, while at high frequencies they act as capacitors. Within a certain frequency range, from 100 to 0.1 s^{-1}, for Mg1.5–55 at 640 °C (Fig. 4), the impedance is quite constant. This range is dominated by R_1, which can be determined with high accuracy (±1%). The attributed phase angle at high frequencies, however, is not −90° as it should be for the ideal case, but somewhat larger (−80°). This is usually explained [26] by dielectric losses which are taken into account by the impedance element "capacitor loss" used for the simulation. Both resistance and phase angle curves shift to higher frequencies with increasing temperatures.

The specific conductivities of the samples were calculated from the respective resistivity R_1 using Eq. (3)

$$\sigma = \left(\frac{1}{R_1}\right)\left(\frac{l}{A}\right) \tag{3}$$

where l/A (thickness/area) is the corresponding geometric factor of each sample.

The Arrhenius plot ($\log\sigma = \log\sigma_0 - E/2.3\,kT$) from 400 °C to temperatures close to T_g is shown in Fig. 5. The conductivity (σ) at 600 °C is equal to $(5.6 \pm 0.3) \times 10^{-9}$ S cm^{-1} for Zn1.5–50 and $(6.3 \pm 0.3) \times 10^{-9}$ S cm^{-1} for Mg1.5–55, with activation energies of 0.86 ± 0.02 eV for Zn1.5–50 and 0.93 ± 0.02 eV for Mg1.5–55.

Homogeneous silicate glasses are usually alkaline ion conductors although in the present case, alkaline earth ions and Zn^{2+} are likely to be the charge carriers. It is still not clear if ionic diffusion and transport in glass is primarily a *vacancy* or an *interstitial* process. The Anderson Stuart [27] and Funke [28] theories propound a *vacancy* mechanism, where it is assumed that the primary process is the jumping of a catión into a nearby (equivalent) site. In contrast, the Elliot model [29] must be interpreted as an *interstitial* mechanism, since the jumping process is itself triggered by the arrival of an additional cation.

It could be argued that the interstitial mechanism would be favoured by a homogeneous glass structure, where the extra cation is free to trigger ionic motions in all directions. On the other hand, if cationic motion is channelled along predetermined pathways, then the free flow of ions will only occur if these are not blocked.

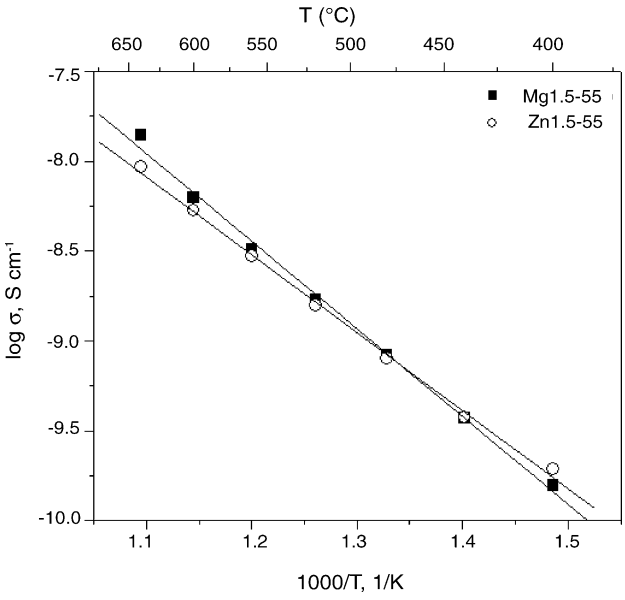

Fig. 5. Arrhenius plots measured from 400 to 640 °C for Mg1.5–55 and Zn1.5–50.

Schlenz et al. [30] have studied the structure of Ba-silicate glasses with 33.3–37 mol% BaO. They propose that [SiO_4] tetrahedra do not exclusively form six-member rings, but also form a considerable number of smaller rings arranged in slightly folded layers which alternate with barium layers and/or barium chains. Additionally, the occurrence of tetrahedral chains, possibly isolated rings, and of regions in which the [SiO_4] tetrahedra form a silica-like network is assumed. Such a structure may favour the vacancy motion mechanism.

Fig. 6(a and b) shows the $\log\sigma$ versus $1/T$ plots for samples Zn1.5–50 and Mg1.5–55 during heating from 500 to 850 °C at heating rates of 2 and 5 °C min^{-1} with isothermal treatment at 850 °C for 15 h, followed by further cooling at the same rates. These results correspond to the second series of measurements carried out at a fixed frequency of 533 mHz. According to the Bode diagrams, at this frequency, the phase angle was dominated by the resistive part of the sample at all temperatures for both samples. The conductivity varies from 7.63×10^{-10} S cm^{-1} at 500 °C to 1.49×10^{-6} S cm^{-1} at 808 °C for Zn1.5–50 and from 1.72×10^{-9} S cm^{-1} at 500 °C to 1.42×10^{-6} S cm^{-1} at 842 °C for Mg1.5–55 both at 5 °C min^{-1}. Thus, the resistance, is much higher than 10^4 Ω cm throughout the temperature range, demonstrating that the materials behave as insulators.

From Fig. 6(a and b), it can be noted that up to temperatures around 640 °C the temperature dependence of conductivity σ is linear. As the temperature rises permitting structural rearrangements, the conductivity starts to deviate from Arrhenius-like behaviour, increasing more rapidly leading to a shorter Arrhenius region with a higher activation energy. This slope change, usually assigned to glass transition phenomena, is reinforced in this case by the reduction of porosity (sintering process) taking

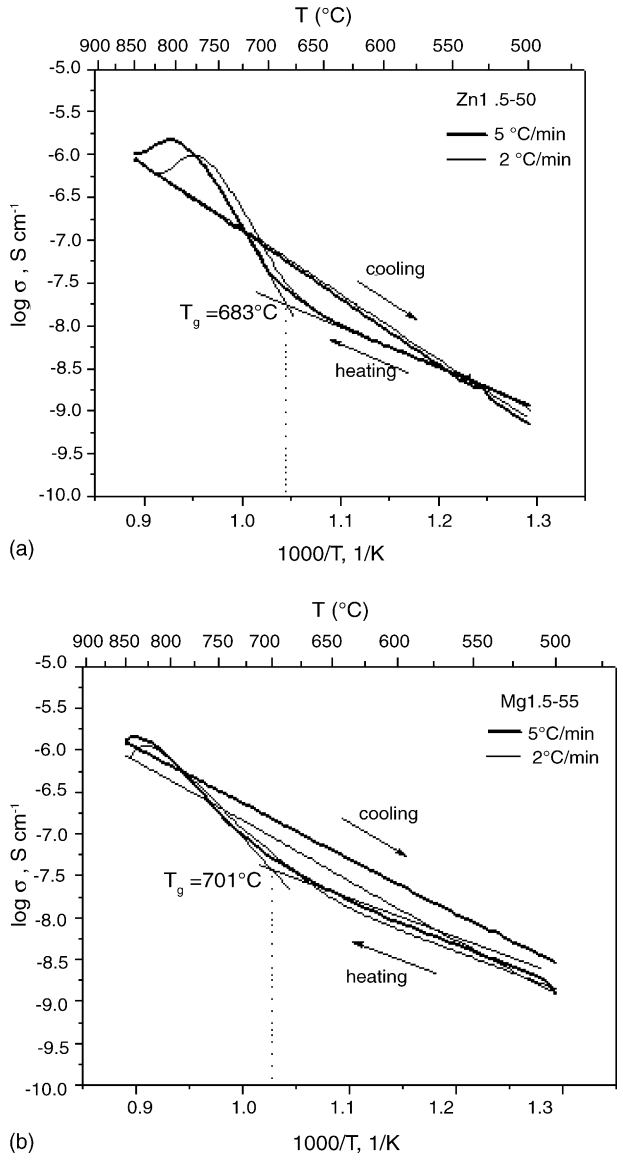

Fig. 6. Arrhenius plots for: (a) Zn1.5–50 and (b) Mg1.5–55.

place during heating from $T > T_g$. The intersection between linear regions on the log σ versus $1/T$ plot has been used to determine T_g (Table 2). T_g values obtained by DTA (Table 1) and EIS (Table 2) are in good agreement within the measurement errors shifting towards higher temperatures as heating rate increases.

Above T_g (Fig. 6), conductivity continuously increases until a maximum at temperatures close to crystallisation takes place.

Table 2
EIS temperatures (±9) (°C)

T (°C)	Zn1.5–50		Mg1.5–55	
	2 °C min^{-1}	5 °C min^{-1}	2 °C min^{-1}	5 °C min^{-1}
T_g (Fig. 6)	673	683	673	701
Maxima range (Fig. 7a)	650–770	670–790	650–825	690–840
Minima range (Fig. 7a)	800	826	839	850

Impedance measurements conducted at 850 °C for 15 h showed only slight changes. The isothermal variation of the resistance is negligible within experimental error (±1%); thereby demonstrating the stability of the crystalline phases formed and that no phase transformations take place. The values of σ (S cm^{-1}) range between 10^{-6} and $10^{-6.5}$ for Mg1.5–55 and between $10^{-5.9}$ and $10^{-6.1}$ for Zn1.5–50.

After maintaining the sample 15 h at 850 °C, the conductivity during cooling (Fig. 6a and b) fits an Arrhenius plot with activation energies of 1.5 eV for Zn1.5–50 and 1.3 eV for Mg1.5–55 at 2 °C min^{-1}. XRD patterns at the end of the heat treatment indicate that samples are crystallised and are similar to those performed with HTXRD. The crystalline phases obtained are the same, independent of the heating rate, with a predominance of barium silicates and barium zinc silicate for Zn1.5–50 and, barium silicates and barium magnesium silicates for Mg1.5–55. The activation energies obtained during cooling can be attributed to the final glass–ceramics and are quite similar for the different cooling rates, indicating that the conduction mechanism is the same.

3.3. Sensitivity of impedance measurements to phase transitions

For an ideal glassy ion-conductor, log σ shows a linear dependency with $1/T$ for $T < T_g$ and hence, the derivative is constant and related to the Arrhenius activation energy for ionic conductivity. When a phase transition occurs or a new phase appears, the viscosity behaviour and the transport properties will be affected. As a consequence, the derivative will change with temperature. Thus, the study of the derivative during heating of the curves in Fig. 6(a and b) ($-\mathrm{d}\log\sigma/\mathrm{d}(1/T)$) is of special interest for a better understanding of the glass transition region and sintering and crystallisation processes. For this purpose, the EIS data have been compared with those obtained by DTA and HSM under the same thermal conditions. Fig. 7 shows the derivative curves ($-\mathrm{d}\log\sigma/\mathrm{d}(1/T)$) obtained from EIS along with the DTA and densification curves for Zn1.5–50 at heating rates of 2 and 5 °C min^{-1}.

The derivative of the conductivity exhibits a broad maximum in the temperature range 650–770 °C and 670–790 °C and well-defined minima at 800 and 826 °C for 2 and 5 °C min^{-1}, respectively. Mg1.5–55 (not shown) derivative curves exhibit similar behaviour. Table 2 presents the temperature range over which a maximum occurs and the temperature of the minima obtained from the derivative curves. These data are in good agreement with those presented in Table 1.

The broad maximum in the derivative of conductivity as a function of temperature for Zn1.5–50, Fig. 7, extends from 650 to 790 °C depending on the heating rate. In this range two thermal processes appear: glass transition between 660 and 690 °C and the beginning of the sintering process, with a rapid reduction of porosity. The proximity in temperature of the two phenomena prevents a more accurate assigments of the maximum.

An easier explanation can be found for the minimum of both derivates of the conductivity plots for heating rates of 2 and 5 °C min^{-1}. These sharp minima coincide well with T_x, the onset

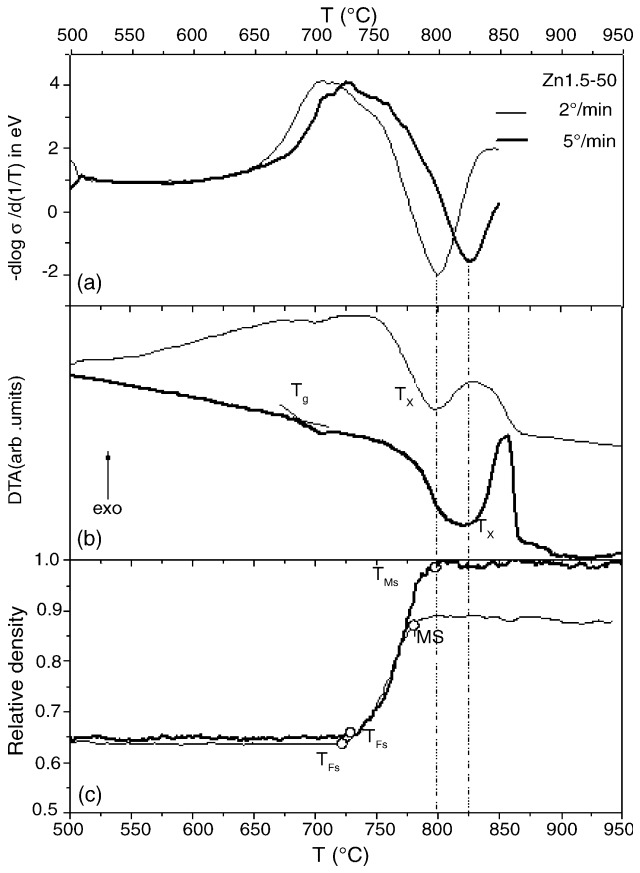

Fig. 7. (a) Derivative curve ($-\mathrm{d}\log\sigma/\mathrm{d}(1/T)$), (b) DTA and (c) sintering of Zn1.5–50 samples.

point for the crystallisation process, indicating the first appearance of crystals in the glassy matrix (compare Tables 1 and 2). It is clear that when this point occurs after T_{MS}, the maximum shrinkage temperature, a dense and homogeneously crystallised glass–ceramic is obtained at the end of the thermal process. In contrast, when $T < T_{MS}$, the densification stops thus inhibiting further sintering. The earlier appearance of T_x for a slower heating rate results from greater nucleation, leading to incomplete densification.

These results demonstrate the potential of EIS when applied to the study of processes involving microstructure changes, such as glass transition or crystallisation.

4. Conclusions

Electrochemical impedance spectroscopy (EIS) was used to characterise the electrical behaviour of glass–ceramics in the systems, RO–BaO–SiO_2 (R = Mg, Zn,), at the temperatures relevant for SOFC operation. The samples are insulators, exhibiting electrical resistances much higher than $10^4\ \Omega\,\mathrm{cm}$ in the range studied of temperatures.

For an ideal glassy ion-conductor, $\log\sigma$ shows a linear dependency with $1/T$ for $T < T_g$. When a phase transition occurs or a new phase, the viscosity behaviour and the transport properties will be affected. In consequence, the derivative ($-\mathrm{d}\log\sigma/\mathrm{d}(1/T)$) changes with temperature. A broad maximum in the derivative of conductivity is related to the range of the glass transition and the beginning of the sintering process. The proximity in temperature of both phenomena prevents a more accurate assignment of the maximum.

On the other hand, the sharp minima obtained coincide well with T_x, the onset point for crystallisation process, indicating the first appearance of crystals in the glassy matrix. When this point situates after T_{MS}, the maximum shrinkage temperature, a dense and homogeneously crystallised glass–ceramic is obtained. In contrast, when $T < T_{MS}$, the densification stops thus inhibiting further sintering. The role of nucleation in the advance occurring of T_x for slower heating rate is the origin of this uncompleted densification. The earlier appearance of T_x for a slower heating rate results from greater nucleation, leading to incomplete densification.

The EIS results are in good agreement with DTA and HSM analysis made in the same thermal conditions. EIS has confirmed its potential for investigating thermal processes in glasses.

Acknowledgement

This work was funded by the research project CICYT MAT 2003-0952-C02-01.

References

[1] N.Q. Ming, J. Am. Ceram. Soc. 76 (1993) 563–588.
[2] K.L. Ley, M. Krumpelt, R. Kumar, J.H. Meiser, I. Bloom, J. Mater. Sci. 33 (1996) 1489–1493.
[3] K. Eichler, G. Solow, P. Otschik, W. Schaffrath, J. Eur. Ceram. Soc. 19 (1999) 1101–1104.
[4] S.B. Sohn, S.H. Oh, S.Y. Choi, G.H. Kim, H.S. Song, J. Korean Ceram. Soc. 38 (2001) 158–165.
[5] P.H. Larsen, P.F. James, J. Mater. Sci. 33 (1998) 2499–2507.
[6] E. Monreal, R. Späh, D. Stolten, DVS-Beritche. 184 (1997) 217–219.
[7] P. Gease, I. Kreutzer, R. Conradt, CD Proccedings, Glass Odyssey Sixth ESG Conference, June 2–6, Montpellier, France, 2002.
[8] N. Lahl, D. Bahadur, K. Singh, L. Singheiser, K. Hilpert, J. Electrochem. Soc. 149 (2002) A607–A614.
[9] C. Lara, M.J. Pascual, M.O. Prado, A. Durán, Solid State Ionics 170 (2004) 201–208.
[10] C. Lara, M.J. Pascual, A. Durán, J. Non-cryst. Solids 348 (2004) 149–155.
[11] K.C. Sobha, K.J. Rao, J. Non-cryst. Solids 201 (1996) 52–65.
[12] B. Munro, B. Wang, M. Greenblatt, J. Non-cryst. Solids 196 (1996) 291–296.
[13] C. Ravagnani, R. Keding, C. Rüssel, J. Non-cryst. Solids 328 (2003) 164–173.
[14] R. Muchillo, E.N.S. Muchillo, Y.V. França, C. Fredericci, M.O. Prado, E.D. Zanotto, Mater. Sci. Eng. A 352 (2003) 232–239.
[15] F. Munoz, R. Keding, C. Rüssel, R. Marchand, A. Durán, L. Pascual, Phys. Chem. Glasses., in press.
[16] K.K. Evstrop'ev, V.A. Kharĭyuzov, Dokl. Akad. Nauk. SSSR 136 (1961) 140–142.
[17] J. Zarzycki, in: J.A. Prins (Ed.), Physics of Non-crystalline Solids, North Holland Publishing Co., Amsterdam, 1965, p. 525.
[18] J.M. Schwartz, J.D. Mackenzie, J. Am. Ceram. Soc. 49 (1966) 582–585.
[19] M. Malki, P. Echegut, J. Non-cryst. Solids 323 (2003) 131–136.
[20] M. Schwartz, Thesis, Rensselaer Polytechnic Institute, Troy, NY, 1969.
[21] O. Kanert, P. Küchler, D. Suter, G.N. Shanon, H. Jain, J. Non-cryst. Solids 274 (2000) 202–207.
[22] R. Keding, D. Tauch, C. Rüssel, J. Non-cryst. Solids 348 (2004) 123–130.

[23] X. Wang, P. Xiao, J. Eur. Soc. Ceram. 22 (2002) 471–478.
[24] M.J. Pascual, A. Durán, L. Pascual, J. Non-cryst. Solids 306 (2002) 58–69.
[25] M.J. Pascual, M.O. Prado, A. Durán, Phys. Chem. Glasses, 2005 (October issue).
[26] B. Rinn, W. Dieterich, P. Maass, Philos. Mag. B 77 (1998) 1283–1292.
[27] O.L. Anderson, D.A. Stuart, J. Am. Ceram. Soc. 37 (1954) 573–579.
[28] C. Funke, Solid State Ionics 28–30 (1988) 100–107.
[29] S.R. Elliot, Solid State Ionics 27 (1988) 131–149.
[30] H. Schlenz, A. Kirfel, K. Schulmeister, N. Wartner, W. Mader, J. Non-cryst. Solids 297 (2002) 37–54.